JOURNAL OF MATERIALS SCIENCE 33 (1998) 2781–2794

# The nature of localized deformation in 6111-T6 aluminium alloy and polycarbonate

M. M. TATA, J. S. OH, D. LEE
*Department of Mechanical Engineering, Rensselaer Polytechnic Institute, Troy, NY 12180-3590, USA*
*E-mail: leed@rpi.edu*

The nature of localized deformation that occurs both in metal and polymer samples was examined under uniaxial tension by measuring the complete strain distribution of a deforming specimen at a constant crosshead speed. The development of localized deformation in 6111-T6 aluminium alloy and polycarbonate was recorded along both the longitudinal and lateral directions as the specimen was stretched until it fractured. Determination of the true strain at various points on the tensile specimens was made by using an automated, vision-based image processing method using a CCD camera to measure the deformation of a silk-screened grid on the specimen. This vision-based system produced accurate results, allowing for careful analysis of the entire necking process from initiation to propagation. It has been observed that localized deformation develops principally in the longitudinal direction. The major and minor true strain are uniform for the uniform section specimens, however, these strains peak in the centre of the hourglass specimens in the longitudinal direction for both materials. For both specimen geometries, the major strain is uniform while the minor strain is non-uniform in the lateral direction. The longitudinal true strain to lateral true strain ratio remains at about two for the uniform section specimens, but this ratio increases to between 3 and 5 for the hourglass specimens, due to the constraining effect of the sample geometry. 

## 1. Introduction

Necking or localized deformations [1] occur both in polymer and metal materials under uniaxial tensile loading conditions, but their behaviours are different, as are their mechanisms. Crazes or voids develop and molecules stretch in amorphous polymers [2, 3], while shear bands develop in metal alloys [2]. Crazes can be regarded as localized, wedge-shaped, narrow regions of highly deformed material [3] or as an assembly of 'micro necks' [4]. Shear bands can be described as localized deformations that develop under the plane strain condition in which there is no contraction along the length of the specimen, but its thickness decreases [2]. These crazes and shear bands are developed during the necking process in the polymer and metal, respectively. Experimental observations of such localized deformation or necking behaviour are important for both understanding the necking phenomena and also for modelling and constitutive equation development [5].

Comprehensive sets of true stress–strain data accompanied by time-lapse photographs depicting the neck initiation and propagation processes are currently not readily available for the thorough understanding and development of constitutive models for polymers [6]. Necking in aluminium and other metals develops in a complex manner where diffuse necking is followed by localized necking [7]. To obtain a more thorough understanding of these materials, 6111-T6 aluminium alloy and polycarbonate injection moulded sheet samples have been examined in this work.

Specifically, and effort was made to understand the phenomenology of localized deformation and to determine if distortion is uniform both in the longitudinal and lateral directions. Previous vision-based surface strain measurement experiments have been performed to determine localized deformation behaviour in the longitudinal direction [6], but no testing of the distortion uniformity in both the lateral and longitudinal directions have been made. The similar experimental method to that used by Haynes and Coates [6] was modelled for this uniaxial testing experiment, but was modified to include strain measurements in both directions. The examination of images in a time series enables the calculation of mechanical properties as well as an accurate description of the complex deformation that takes place with increasing strain along the longitudinal and lateral directions.

The determination of the strain at various points on the tensile specimens was performed by using the method developed by Manthey and Lee [8] to measure surface strains and to observe neck initiation and growth phenomenon in both the longitudinal and

0022–2461  

the lateral directions. The photogrammetric measurement simulation program produces a set of images based on the accuracy of the charge-coupled device (CCD) camera and the size of the grid on the sample. By using two geometries of specimens, and two crosshead speeds for testing, true stress–true strain relationships have been obtained that are valid for 6111-T6 aluminium alloy and polycarbonate at various testing speeds to the point of failure. Temperature does affect the deformation process, but this was not examined in this experimentation. All tests were performed at room temperature.

One observation is that necking initiates and propagates in solely the longitudinal direction for polycarbonate and fracture occurs normal to the longitudinal axis. Necking initiates and propagates at an angle of between 68 and 78° from the sample's longitudinal (tensile) axis in the 6111-T6 aluminium. This fracture angle is greater than the typical 55°, probably because the aluminium is slightly anisotropic in the plane of the sheet [3, 7]. Another observation is that the longitudinal true strain to lateral true strain ratio remains at about two for the uniform gauge section specimens, but this ratio increases to between 3 and 5 for the hourglass specimens, due to the constraining effect of the initial sample geometry. The major and minor true strains in the longitudinal direction are uniform for the uniform section specimens, but peak at the centre of the hourglass specimens. For both sample geometries, the major true strain is uniform and the minor true strain is non-uniform in the lateral direction.

## 2. Experimental and analytical methods

### 2.1. Test samples

Numerous tensile tests have been made with 6111-T6 aluminium alloy and polycarbonate. An aluminium alloy was chosen as a metal that has a limited ductility and tends to develop localized deformation. Polycarbonate was selected as a representative engineering plastic that is ductile, but which exhibits inhomogeneous localized deformation. The test specimens for the aluminium were cut from rolled sheets. The polycarbonate test specimens were machined from injection moulded sheet. It was expected that the polycarbonate would develop strains that were much higher than those for the 6111-T6 aluminium alloy.

The 6111-T6 aluminium alloy specimen thickness was 0.932 mm and that of the polycarbonate was 1.613 mm. Both the uniform and the hourglass specimens were 152.4 mm in length with a width of 25.4 mm in the shoulder area. For the uniform section specimens, the gauge length was 50.8 mm with a 12.7 mm radius from the shoulder area. The width of the gauge section area was a constant 12.7 mm. For the hourglass specimens, the area between the two shoulders was machined to a radius of 50.8 mm. The distance between the shoulders was 50.8 mm with a minimum width of 11.12 mm in the centre of this curved area for the hourglass specimens. The long gauge length of these specimens was specifically chosen to allow the investigation of neck propagation. The neck was found to reach the shoulders more rapidly after neck initiation, in specimens with shorter gauge lengths in both the uniform section [6] and hourglass specimens [5].

Both uniform section and hourglass specimens were tested because they complement one another. With uniform section specimens, the exact location of necking cannot be determined prior to testing because the entire gauge length has the same width. For the hourglass specimens, the minimum width was machined to be in the exact centre of the reduced area between the shoulders. The extensometer was placed at this minimum width. Necking almost always occurs at this minimum width; therefore, the extensometer results are valid until the sample breaks for the hourglass specimens. Previous experimentation [9], showed that because the neck growth behaviour is dependent on specimen geometry, the stress–strain curve obtained from the uniform gauge section specimen deviated from that of the hourglass specimen.

Although much work has been reported on the use of automated grid analysis methods to measure the strains in metals undergoing tensile and compressive deformation, little has been published on this method applied to polymers, where the strains are much higher and cause distortion of the marked grid [6]. A black square grid of 1.270 mm (0.05 inch) was applied to the entire surface area on one side of all of the specimens using a silk-screening method. The maximum number of grid intersection points was utilized so that strain values across the lateral and longitudinal directions of the specimens could be obtained. The average width and height of the square grid on the samples were measured to be 1.274 mm and 1.270 mm, respectively.

### 2.2. Mechanical testing

The basic tools used for the experiment were an Instron Test Machine Floor Model 4204, a 12.5 mm gauge length extensometer, a frame grabber, and the ASAME (automated strain analysis and measurement environment) vision-based surface strain measurement system [10]. The LabVIEW [11, 12] program was also utilized for data gathering and for generating plots of the data. Simultaneously, one computer was used for gathering the data for the ASAME program and another computer was utilized to gather the data using LabVIEW. A CCD camera was used in conjunction with the ASAME program [10] to gather the images of the specimen and it was stretched and deformed in tension. The camera was positioned in front of the specimen and focused, then it remained stationary throughout the testing process. Fig. 1 shows the set up of the experiment with the Instron machine, one of the computers utilized, and the CCD camera. Extra lighting was also used to enhance the colour contrast between the grey/silver colour of the samples and the black grid lines.

Several steps are involved in the vision-based method utilized in this experimentation. First, the frame grabber captures the image at specified time intervals through the CCD camera. Once all of the

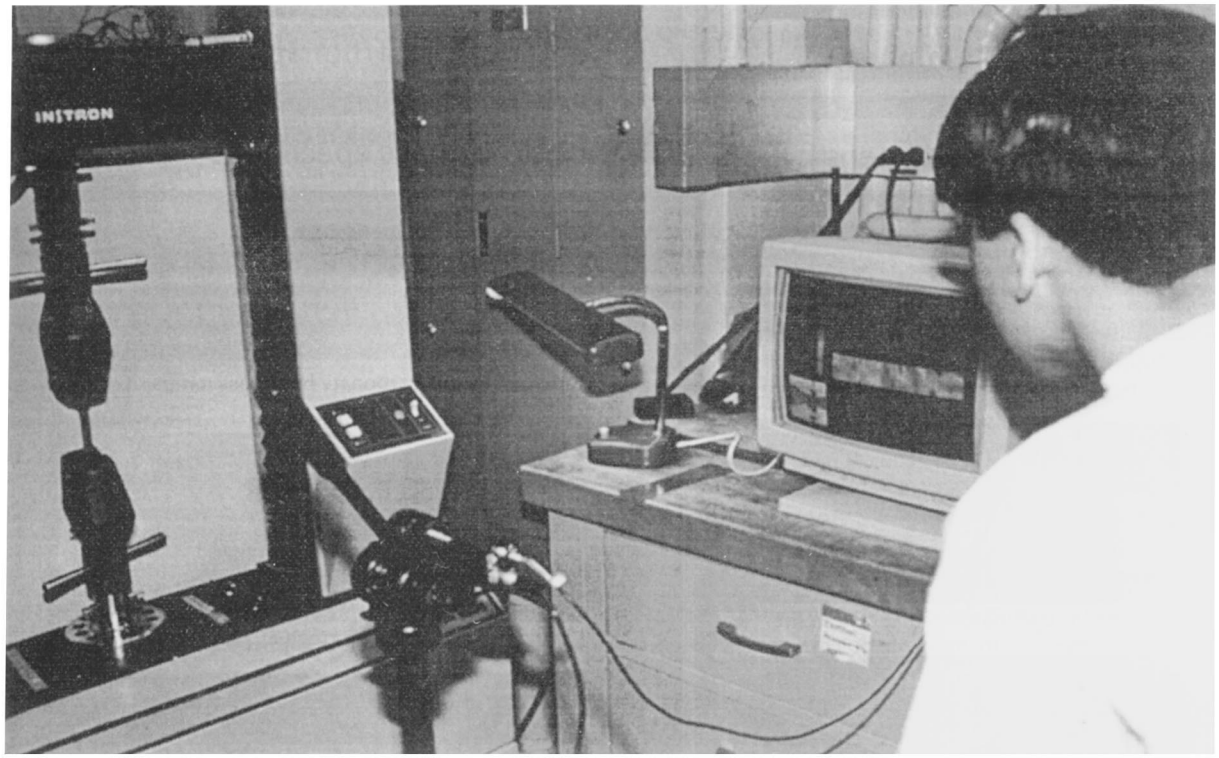


*Figure 1* Testing equipment and set-up including Instron testing machine, CCD camera, and computer running ASAME program.

TABLE I Details of testing performed including quantities of specimens tested for each material, geometry, speed and measurement method

| Specimen material | Specimen type | Slow speed samples | Fast speed samples | Extensometer |
|---|---|---|---|---|
| 6111-T6 aluminium | Hourglass | Two (10 mm min$^{-1}$) | One (25 mm min$^{-1}$) | Yes |
| 6111-T6 aluminium | Hourglass | Two (10 mm min$^{-1}$) | None | No |
| 6111-T6 aluminium | Uniform | Two (25 mm min$^{-1}$) | One (62.5 mm min$^{-1}$) | No |
| Polycarbonate | Hourglass | Two (10 mm min$^{-1}$) | One (25 mm min$^{-1}$) | Yes |
| Polycarbonate | Hourglass | Two (10 mm min$^{-1}$) | None | No |
| Polycarbonate | Uniform | Two (25 mm min$^{-1}$) | One (62.5 mm min$^{-1}$) | No |

images have been collected by the ASAME program [10], the user defines the deforming area for the strain analysis. An image often requires patching by the user to ensure that the grid lines are unbroken. The patches can correctly recreate the grid lines because the original image of the sample can be displayed on the screen simultaneously. Then, the user can simply trace the original grid lines, that may have disappeared in some areas during the filtering stage, by connecting the start and end points of the line. The next step is the application of a line thinning algorithm, which reduces each line to a width of one pixel, while maintaining continuity [13]. Finally, the strain for each grid intersection point is calculated by the ASAME program [10].

A fast and a slow speed were used to test each of the two types of specimens, for both 6111-T6 aluminium alloy and polycarbonate, to ensure that the experimental results were valid for various testing speeds. None of the uniform section specimens were tested with an extensometer because the extensometer would have prevented the viewing of the sample with the camera. Also, there is no accurate means of predicting where necking will initiate on the uniform section specimens. Nonetheless, some of the hourglass samples were tested using a spring loaded transverse extensometer, so that the data obtained experimentally from the extensometer could be compared to the vision-based measurements. Table I shows the quantity of samples tested for each material, geometry, speed, and whether or not an extensometer was used. The uniform section specimens were tested at a speed that was a factor of 2.5 faster than that of the hourglass specimens because the uniform section samples have a greater minimum width in the area between the shoulders.

Fig. 2 shows undeformed samples and deformed samples pulled at a slow speed without the extensometer, for both the hourglass and the uniform section specimens. These slow speeds are 10 mm min$^{-1}$ for the hourglass samples and 25 mm min$^{-1}$ for the uniform gauge section samples. Fig. 2a shows the 6111-T6 aluminium specimens and Fig. 2b shows the polycarbonate specimens. Fig. 2a shows that the aluminium specimens consistently fractured at an angle of approximately 70° from the longitudinal axis and

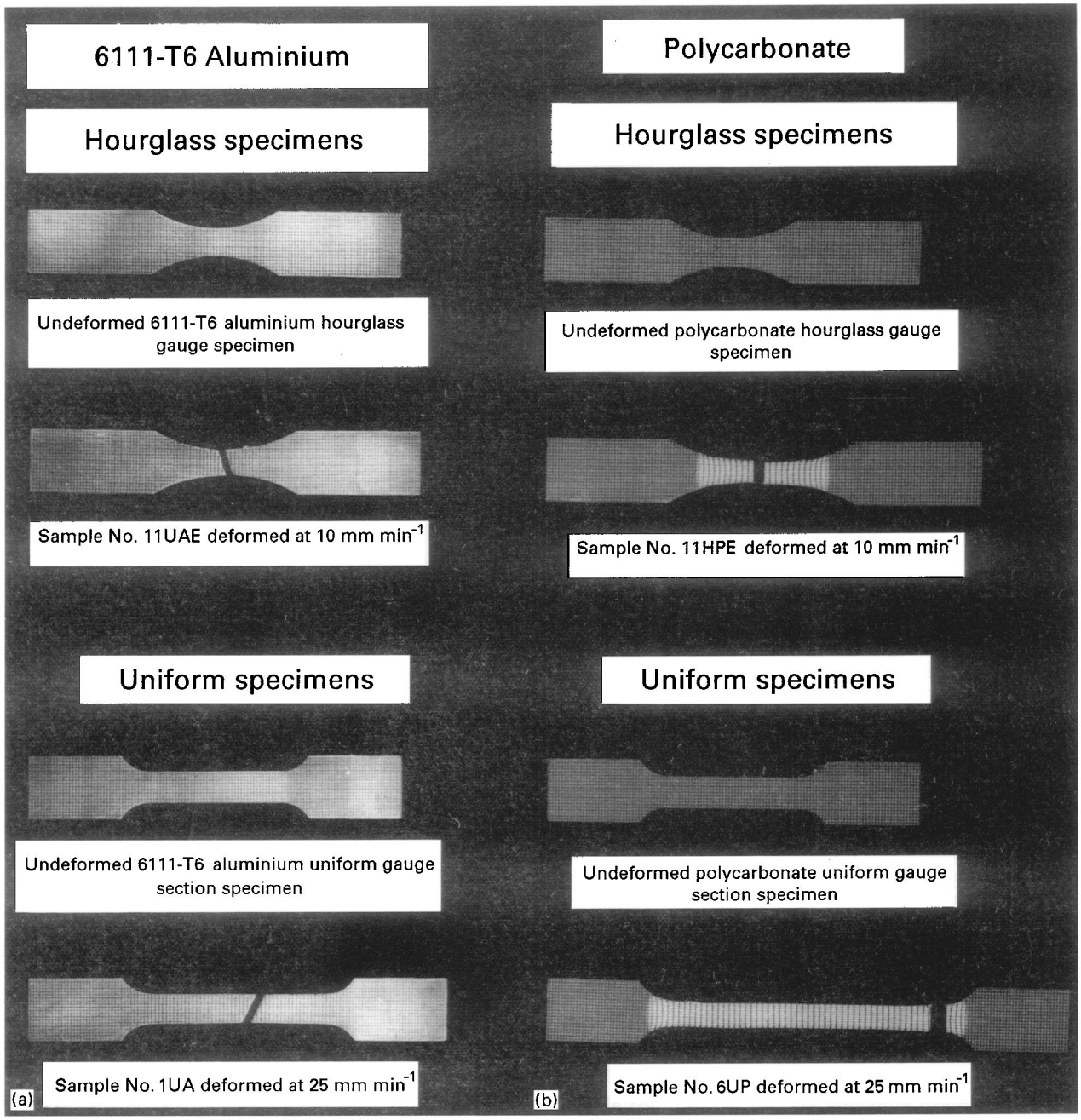


*Figure 2* (a) 6111-T6 aluminium hourglass and uniform gauge specimens undeformed and deformed without an extensometer, (b) polycarbonate hourglass and uniform gauge specimens undeformed and deformed without an extensometer.

that these specimens did not elongate very far before they fractured. Fig. 2b shows that the polycarbonate specimens consistently fractured at an angle of about 90° from the tension axis and that the specimens elongated quite far before fracture.

## 2.3. Image acquisition and processing

For this experiment, simple image processing was chosen over the traditional photographing and film development followed by image grabbing [8, 14]. The benefits of the image processing procedure over traditional methods have been cited by others [14–16], as including high automation, full-field measurement, central processing unit time reduction, and subpixel registration. The ease of use, accuracy, and ability to measure strain in both the lateral and longitudinal direction enable the vision-based system used in this experimentation to surpass even the more current vision systems.

During the experiment, numerous digital images of the specimen were captured at specified time intervals. Using the ASAME program [10], as many as 100 images can be acquired and stored for each specimen. However, since each image needs to be processed individually, five to seven images were actually taken for each sample to adequately depict the stages of neck initiation and growth. The camera was positioned such that the deforming area would remain on the computer screen while the sample was stretched in tension. The images were focused to contain the area between the shoulders of the specimens across the

entire viewing area of the camera, so that the grid lines were visible as much as possible on the computer images. This maximum amount of deforming area was captured with the CCD camera so that a more comprehensive analysis of the strain distribution could be obtained. The first image always represented the sample before any load was applied to it. For most of the samples, the time interval was defined such that the final image was taken of the specimen after fracture. The images were processed after the uniaxial tensile test was completed.

### 2.4. Finite element analysis

Experimental data are compared against the results obtained from the numerical modelling method. The finite element analysis (FEA) was conducted using the same geometry and testing conditions for the uniaxial test of the polycarbonate specimen. Taking advantage of the symmetric geometry of the hourglass specimens, only one quarter of a tensile specimen is modelled for FEA [15, 17]. However, this makes it necessary to use appropriate boundary conditions for FEA. For instance, the displacement for the FEA model is set to be at half of a particular crosshead displacement found in the experiment. Also, this FEA model is based on the plane stress boundary condition. The input stress–strain curve for FEA is approximated as a piece-wise continuous curve fitted to previously published experimental data [5, 7].

## 3. Results

### 3.1. Comparison of strain measurement methods and stress–strain relationship

For the results obtained from the extensometer, it was assumed that both the 6111-T6 aluminium and the polycarbonate are isotropic and maintained a constant volume [6, 9] throughout the test. Based on these assumptions, the strain in the longitudinal direction is equivalent to twice the compressive strain in the lateral width and thickness directions. Also, the lateral width and thickness strains are equivalent. For the vision-based analysis, only the constancy of volume assumption was utilized.

Two predominant issues have been examined in this experimental work. The first is whether or not the vision-based method gives correct strain measurement. The second is a validation of whether or not the longitudinal true strain is indeed equal to twice the lateral true strain, verifying the isotropy and the constancy of volume assumption as well as the role of the geometrical constraining effect. Experiments, using an automated grid analysis method, performed by Sirkis and Lim [16], showed that the average strains were consistently higher than the normal strain provided by the strain gauge, while the shear strains were still close to zero. This discrepancy was attributed to some out-of-plane rigid body motion that takes place during loading.

One potential problem with the stress–strain curve for the polycarbonate is that it does not correctly depict the actual response of the plastic to the applied stress because the deformation will generally be localized in the form of a neck, which may then be propagated through the test piece [4]. The resulting stress–strain curve may not correctly reflect the actual response of the material to the applied stress. To account for this problem, the true strain data were taken along the width of the specimen, at the location where necking occurred, using the extensometer. When the vision-based system was used, it did not matter where necking occurred because the strain results accurately depict areas of deformation.

The first set of plots, Fig. 3a and b, compares the vision-based major and minor true strain measurement data against the extensometer data across the lateral direction of the hourglass specimens for 6111-T6 aluminium and polycarbonate samples, respectively. In the lower portion of both plots, the extensometer strain data are compared directly with the average and peak minor true strains, also known as the width strains. While only one set of minor strain data are obtained from the outer edge of the specimen in the lateral direction using an extensometer, strains at every grid intersection point can be obtained from the vision-based measurement method. This large number of grid points, obtained from the ASAME program [10], created a need for both average and peak strains to be plotted. The results of this plot confirm that the vision-based strain measurement method is consistent with the extensometer data and with previous experimental data [5]. For both 6111-T6 aluminium and polycarbonate samples, the average lateral strain values show a better agreement with the extensometer data than the peak lateral strain values.

The other significant finding of Fig. 3 is that the measured longitudinal true strain using the

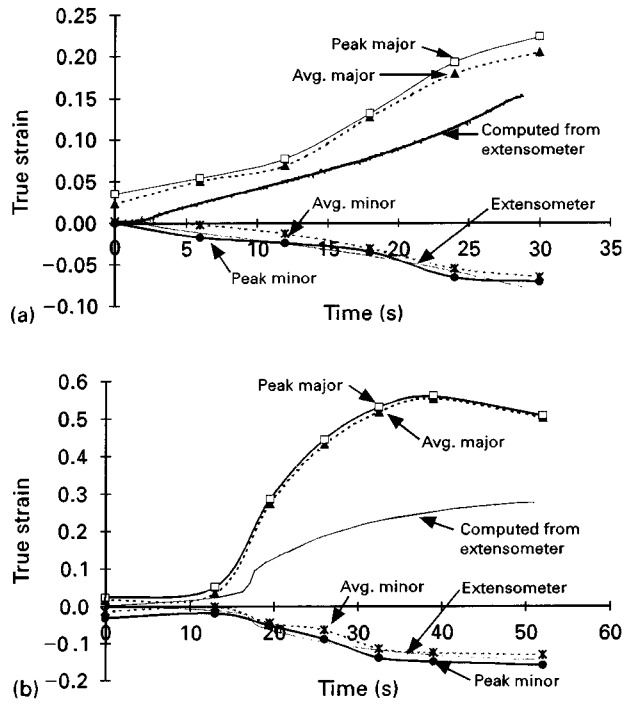


*Figure 3* (a) 6111-T6 aluminium hourglass and (b) polycarbonate hourglass specimens peak and average major and minor true strains taken along the lateral direction from vision-based system and extensometer measurements.

vision-based method is greater than that predicted using the volume constancy and isotropy assumptions, based on the lateral strain as measured by the extensometer. This predicted longitudinal strain is shown as the line labelled "Computed from extensometer" in Fig. 3 and was calculated as twice the lateral strain of the extensometer. The longitudinal to lateral true strain ratio of the hourglass specimens, as determined by the vision-based system, is actually about 3.1:1 for 6111-T6 aluminium and about 5.1:1 for polycarbonate, as can be seen in the cross plot of Fig. 7. The fact that the typical 2:1 longitudinal to lateral strain ratio is maintained in the uniform gauge section specimens and not in the hourglass samples suggests that this observed deviation from the 2:1 ratio is solely due to the constraining effect of the hourglass sample geometry.

True stress–true strain relationships are plotted for both materials in Fig. 4 for the hourglass specimens. Assuming that deformation occurs at constant volume, the actual cross-sectional area of each element can be calculated from the initial volume of the element and the surface strains, allowing the true stress to be calculated from the monitored load and the measured strain [5]. The notch strengthening effect of the hourglass samples was not accounted for in the construction of this stress–strain relationship. Fig. 4a shows the true stress versus true strain results for 6111-T6 aluminium alloy and Fig. 4b those for polycarbonate. Obviously the number of data points obtained from the vision-based method is limited, since only 5 to 7 images were taken for each specimen. In spite of this limitation, the data from the vision-based method give fairly consistent results when compared with the extensometer measurements.

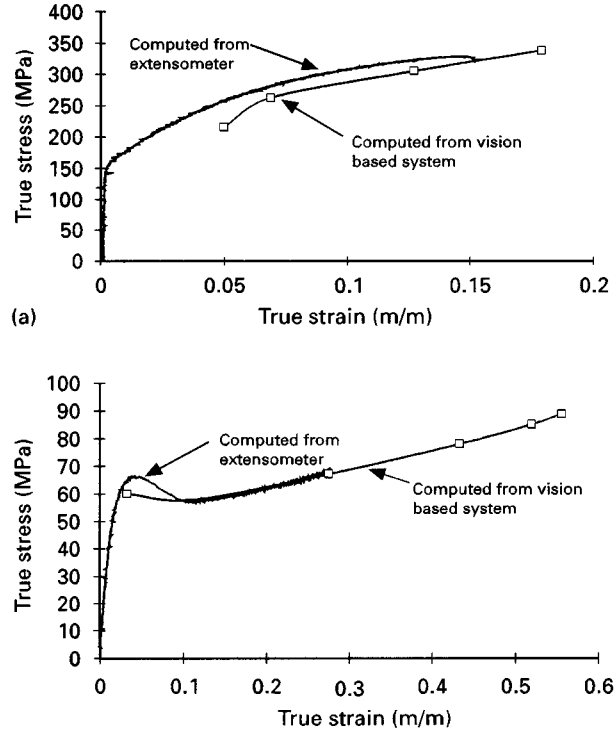


*Figure 4* (a) 6111-T6 aluminium hourglass and (b) polycarbonate hourglass specimens true local stress versus true local strains results in the lateral direction obtained experimentally by vision-based system and extensometer measurements.

## 3.2. Neck development and accompanying strain distribution

Successive stages of deformation showing the initiation and propagation of localized deformation in both sample geometries for 6111-T6 aluminium alloy and polycarbonate are shown in Figs 5 and 6. These figures show the major and minor true strain distribution of the samples. Fig. 5 provides black and white contour drawings and Fig. 6 shows colour contour drawings of the major (longitudinal) and minor (lateral) true strain for each specimen at specific time intervals. The top picture of each specimen is at time zero, before any deformation has taken place. The remaining images sequentially show the specimen as it deforms with time. The longitudinal true strain is the strain along the length of the specimen. The lateral true strain is the strain along the width direction of the specimen.

Fig. 5a and b show the major and minor true strain images for a uniform gauge section specimen, and Fig. 5c and d for a hourglass 6111-T6 aluminium alloy specimen. A neck develops at an angle of about 70° from the longitudinal axis in the aluminium specimen, as it strain hardens uniformly up to the point of maximum load, where fracture takes place. Both uniform and hourglass aluminium samples show such a trend, as shown in Fig. 5. On the other hand, polycarbonate samples develop a well-defined neck with a reduced cross-section, sometimes showing multiple necks, as shown in Fig. 6a. Fig. 6a and b show the images for a uniform section polycarbonate specimen. Fig. 6c and d show the images for a hourglass polycarbonate specimen.

The major and minor true strain values given below for the samples in Figs 5 and 6 were determined by obtaining the maximum and minimum true strain values along one grid line in the lateral direction, through the ASAME program [10]. Fig. 5a and b show that the 6111-T6 aluminium uniform section specimen has a strain distribution at 32 s that varies from 0.19 to 0.21 for the major true strain and from $-0.04$ to $-0.10$ for the minor true strain. Fig. 5c and d show that the 6111-T6 aluminium hourglass specimen has a strain distribution at 24 s of 0.17 to 0.19 for the major true strain and $-0.01$ to $-0.06$ for the minor true strain. Similarly, Fig. 6a and b show that the polycarbonate uniform section specimen has a strain distribution at 150 s that varies from 0.64 to 0.66 and a minor true strain distribution that varies from $-0.32$ to $-0.40$. Fig. 6c and d show that the polycarbonate hourglass specimen has a major true strain distribution at 39 s of 0.54 to 0.56 and a minor true strain distribution of $-0.09$ to $-0.16$. The results for these four particular samples are representative of the results of all the other specimens tested.

The progressive images of Figs 5 and 6 show that the major true strain is more or less uniform across the width of the specimen; however, the minor true strain

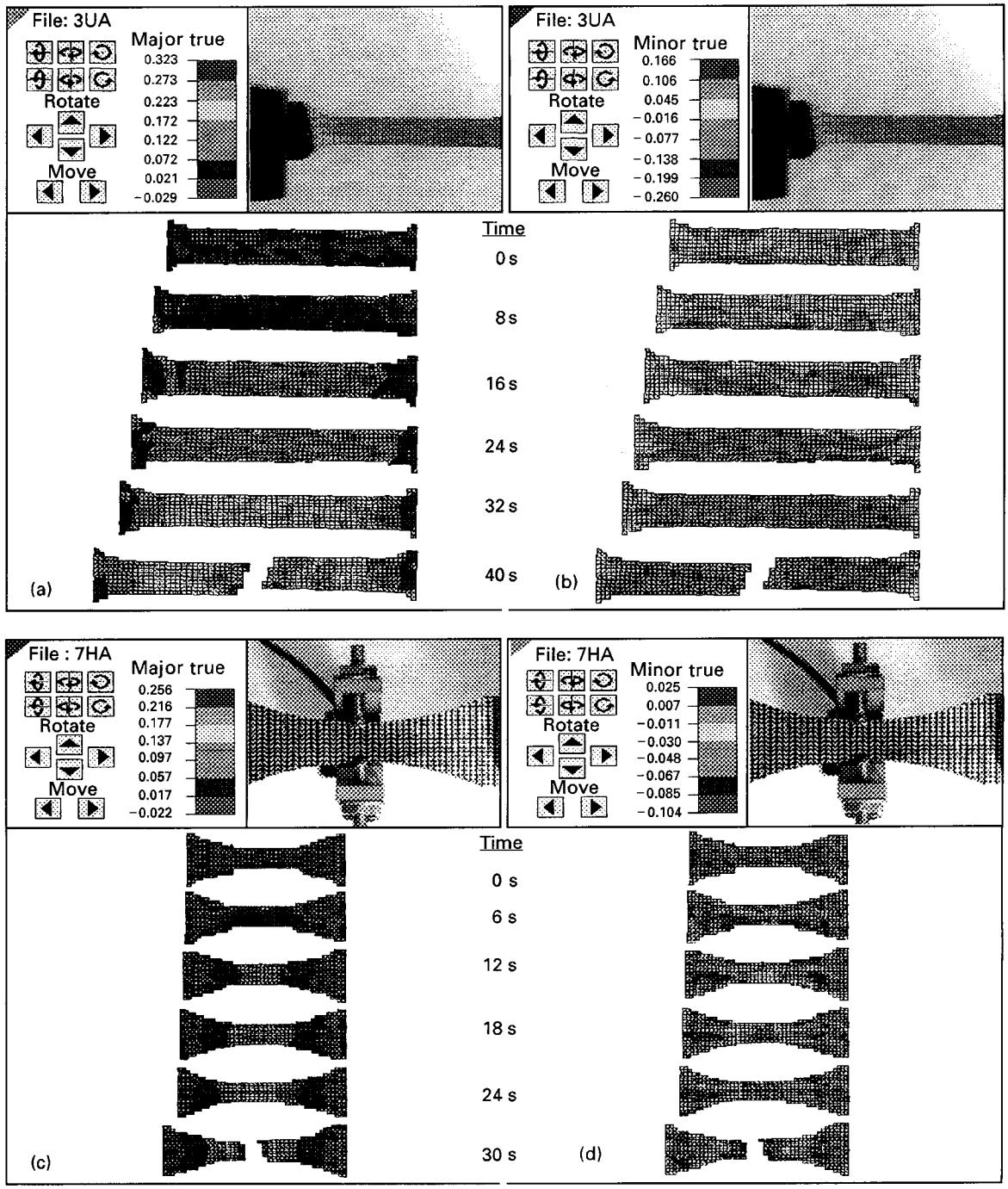


*Figure 5* (a) Longitudinal (major) and (b) lateral (minor) true strain distribution in 6111-T6 aluminium uniform section specimens at specified time intervals, (c) longitudinal (major) and (d) lateral (minor) true strain distribution in 6111-T6 aluminium hourglass specimen at specified time intervals.

tends to be slightly non-uniform across the width of the specimen, as the specimen is deforming, as shown in Fig. 5b and d. The minor true strain is also non-uniform at the transition of the necked and the unnecked region, as can be seen in Fig. 6b. These observations seem to be valid for both the uniform section and the hourglass specimens. More details on true strain distribution can be seen by making cross plots of these figures, as shown in Fig. 7.

Fig. 7 shows cross-section plots of both the major and minor strains across the specimen's centre grid line in both the longitudinal and the lateral directions for a typical 6111-T6 aluminium and polycarbonate specimen, respectively. The major and minor strain values were determined by the ASAME program [10] at each node along the centre longitudinal row of the specimen and along the centre lateral column of the specimen. The cross-section plot represents the strain values of each node at its particular distance along the specimen.

Fig. 7a shows the cross plot for a uniform section and Fig. 7b for a hourglass 6111-T6 aluminium specimen. Fig. 7c shows a cross plot of strains for a uniform specimen and Fig. 7d for a hourglass polycarbonate specimen. It should be noted that both the major and minor true strains, for both materials, reach peak

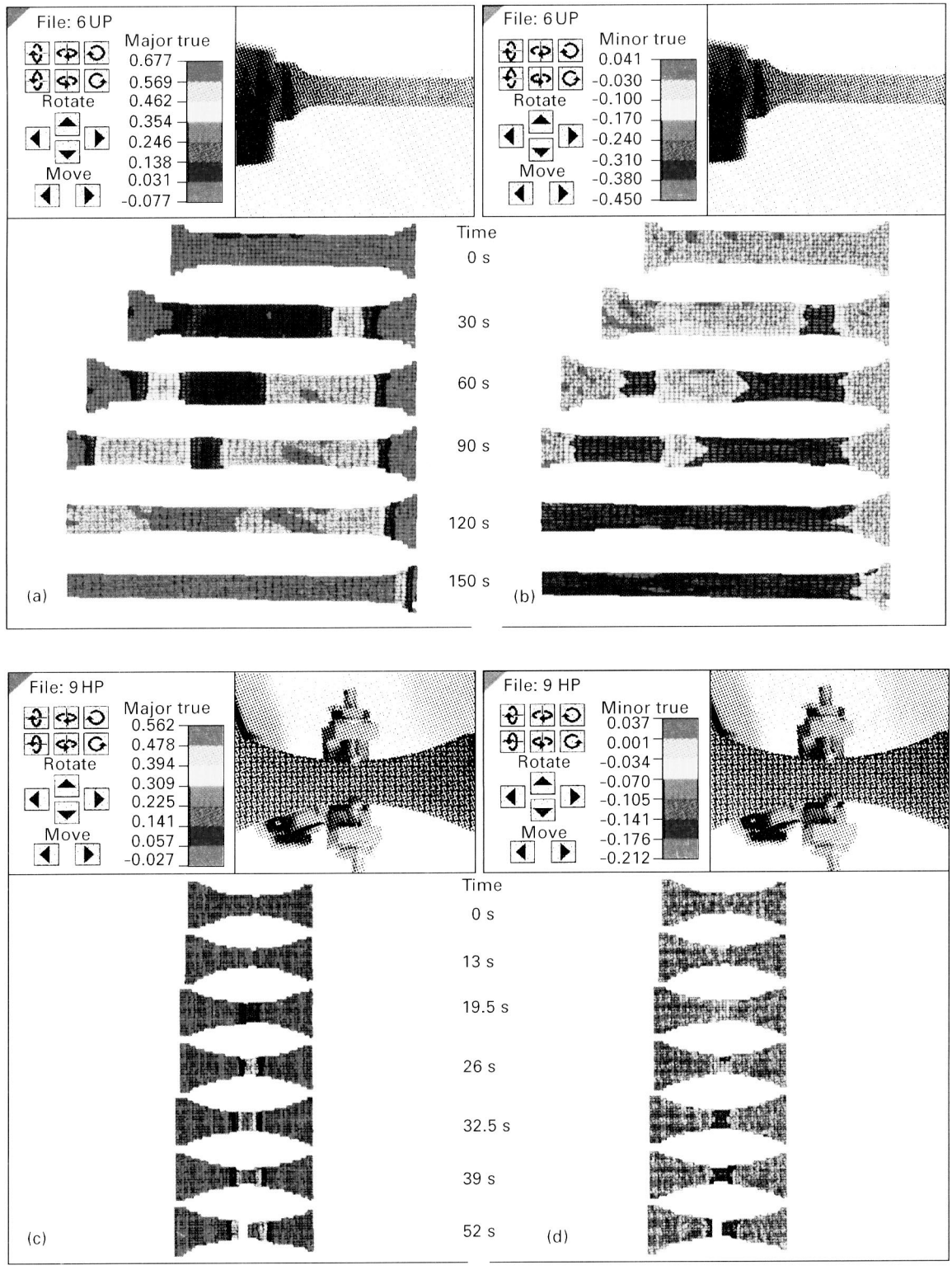


*Figure 6* (a) Longitudinal (major) and (b) lateral (minor) true strain distribution in polycarbonate uniform section specimens at specified time intervals, (c) longitudinal (major) and lateral (minor) true strain distribution in polycarbonate hourglass specimens at specified time intervals.

values at the minimum width of the hourglass sample geometry. Also, it is observed that all the minor strains in the lateral direction formed concave curves on each cross-section plot. The concave curves imply non-uniform strains that peak in the centre of the width of the specimen. These cross plots show that the outer edges of specimen are susceptible to higher minor true strain than the inner part of specimens during the uniaxial tensile test. In contrast, all of the major true strains in the lateral direction, from the cross-section plots, indicate relatively uniform strain.

Fig. 7a shows that the average major true strain in the longitudinal direction for the uniform section 6111-T6 aluminium specimen is approximately 0.17 and the average minor true strain is about $-0.07$. In the lateral direction, the average major and minor true

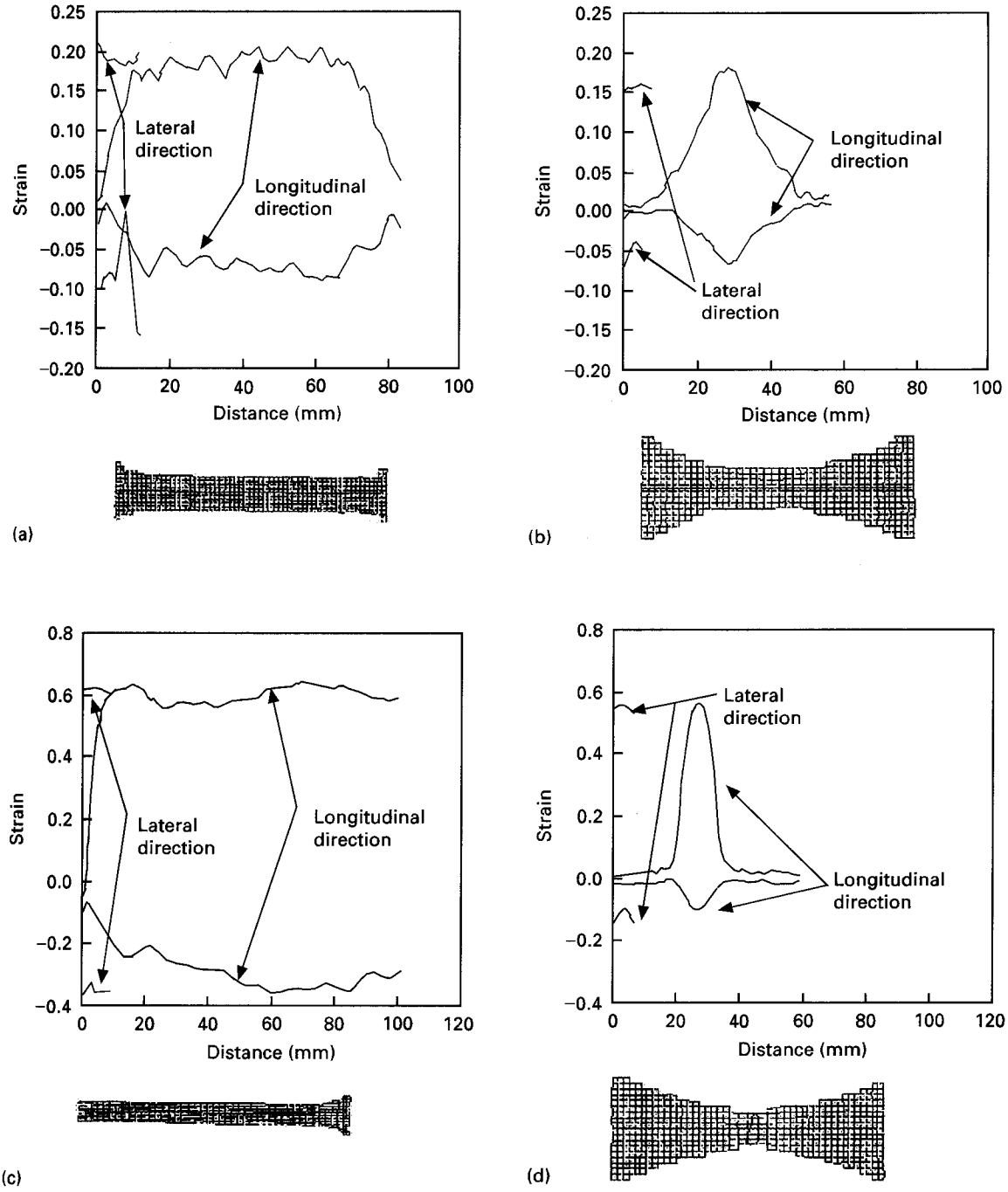


*Figure 7* Cross plot of true major (upper lines) and true minor (lower lines) strains versus distance across centre grid line in the longitudinal and lateral directions for (a) uniform section specimen, and (b) hourglass specimen of 6111-T6 aluminum (c) uniform section and (d) hourglass specimen of polycarbonate.

strains are 0.18 and − 0.08, respectively. These values show that the major true strain to minor true strain ratio is about 2.4 in the longitudinal direction and 2.25 in the lateral direction for the uniform section 6111-T6 aluminium specimens. The peak major and minor true strains are 0.18 and − 0.06 in the longitudinal direction, and the average major and minor true strains are 0.16 and − 0.05 in the lateral direction for the hourglass 6111-T6 aluminium specimen. Overall, the major to minor true strain ratio increases to about 3 in the longitudinal direction and 3.2 in the lateral direction for the hourglass aluminium specimen.

Fig. 7c shows that the average major true strain in the longitudinal direction for the uniform section polycarbonate specimen is approximately 0.60 and the average minor true strain is about − 0.27. In the lateral direction, the average major and minor true strains are 0.64 and − 0.35, respectively. These values show that the major true strain to minor true strain ratio is about 2.2 in the longitudinal direction and 1.8 in the lateral direction for the polycarbonate uniform section specimens. The peak major and minor true strains are 0.56 and − 0.10 in the longitudinal direction, and the average major and minor true strains are 0.55 and − 0.12 in the lateral direction for the hourglass polycarbonate specimen, respectively. Overall, the major to minor true strain ratio increases to about 5.6 in the longitudinal direction and 4.6 in the lateral

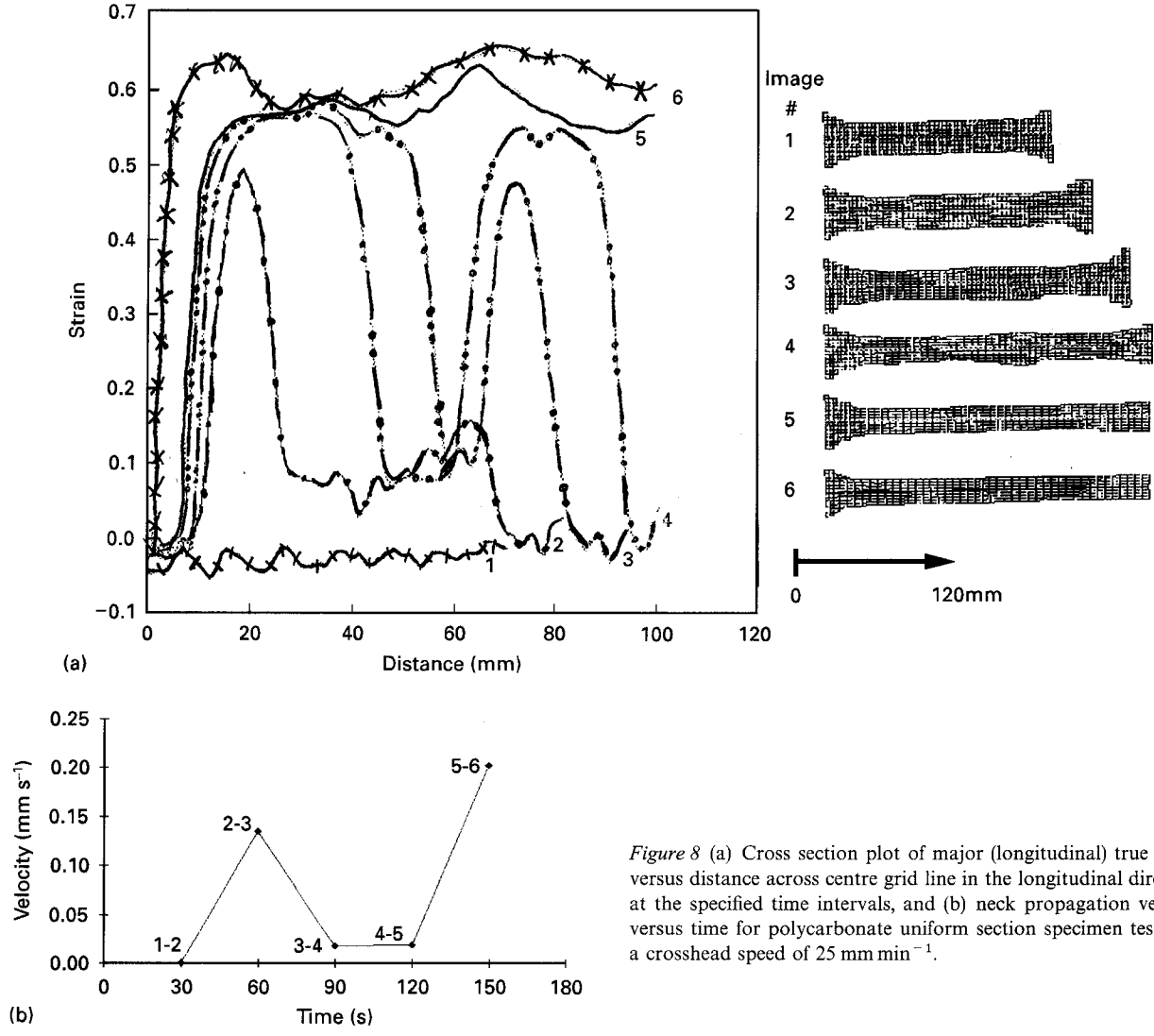


*Figure 8* (a) Cross section plot of major (longitudinal) true strain versus distance across centre grid line in the longitudinal direction at the specified time intervals, and (b) neck propagation velocity versus time for polycarbonate uniform section specimen tested at a crosshead speed of 25 mm $min^{-1}$.

direction for the hourglass polycarbonate specimen. These major and minor true strains results for polycarbonate are consistent with previous work [5].

The ASME program [10] can generate a cross-section plot (strain versus distance) that displays the true strain distribution along a user-defined path on the specimen's surface. Fig. 8a represents six cross-section curves from the six images of the polycarbonate uniform section specimen at the 10 mm $min^{-1}$ testing speed. Each curve represents a major true strain along the middle of the specimen in the longitudinal direction. The left side of the specimen is the origin for the distance on the plot and images 1 and 6 are the first and last image from the uniaxial test, respectively. The distance axis represents the length of the specimen; therefore, the curves extend progressively further to the right from images 1 to 4, because the sample is elongating.

In Fig. 8a, curve 1, which corresponds to image 1, shows approximately zero true strain along the entire distance, because the specimen is not deformed at this stage. Curve 2 shows a distinct neck development and the initiation of a second neck at about 62 mm from the left side of the specimen. The double neck is fully developed and visible in curve 3, and curve 4 shows that two necks are a beginning to merge with each other. While the multiple necks form a single neck (curve 5) and propagate throughout the uniform gauge section area of the specimen, the neck also propagates to the shoulder of the specimen (image 6).

Haynes and Coates [6] measured the neck propagation velocity by the horizontal separation of the strain–time curves, which consisted of individual elements along the uniform section specimen's gauge length. The neck propagation velocity (distance divided by time) was determined from the elemental spacing and the time interval between images. Fig. 8b shows the neck propagation velocity versus time of the same specimen as was used in Fig. 8a. By defining a line in a longitudinal direction of the specimen, the rapid change of strain values along that line (distance), can be seen easily from the cross-section plot when the neck initiates in the specimen. Then, the location of the neck is determined by taking the distance that corresponds to half of the strain between the average high and average low true strain from the cross-sectional plot.

The neck location points, as obtained from the curves, and the time intervals between the images are

used to create the neck propagation velocity versus time plot. Since there is no deformation at image 1, the point 1–2 in Fig. 8b shows zero neck propagation velocity. The point 2–3, which corresponds to curves 2 and 3, shows neck initiation and an increase in velocity to about 0.14 mm $s^{-1}$. The velocity decreases to nearly zero at the points 3–4 and 4–5, where the double neck propagates throughout the uniform section gauge area. The corresponding curves and images of these points show that the left-most location of the neck slows down in speed until the double neck forms a single neck. Then, it starts to propagate to the shoulder of the specimen and the neck propagation velocity increases again to 0.20 mm $s^{-1}$, which is shown at the point 5–6. The average of the neck propagation velocity from the points 2–3 and 5–6 is about 0.17 mm $s^{-1}$. Coates and Ward [18] have proposed an equation to determine the neck propagation velocity in a uniaxial tensile test, involving the crosshead speed and the maximum draw ratio. The neck propagation velocity computed using their equation [18] gave a value of 0.18 mm $s^{-1}$, which agrees well with the value 0.17 mm $s^{-1}$ that is determined from Fig. 8.

## 4. Discussion

The CCD camera acquires images of the specimen at a user specified time interval. The image allows for the contrast between the grey sample and the black grid lines. A measurement of the displacement of the intersection of these grid lines allows the ASAME program [10] to calculate the strain at each point on the specimen.

The images gathered by the ASAME program [10] and CCD camera were post-processed and produce an overall accuracy of $\pm$ 2%. The CCD camera has a resolution of approximately 500 by 500 pixels, horizontal and vertical elements [14]. The extensometer used has an accuracy of 0.5% in its $\pm$ 5 mm deflection range.

Fig. 9 shows a comparison of the experimentally obtained major (longitudinal) strain distribution from the vision-based system and the computer simulated model from the finite element analysis program, ABAQUS [19]. A similar comparison has been made by Coates *et al.* [20]. The hourglass polycarbonate specimen is used for the comparison and 5 mm of displacement is set for FEA boundary condition, which is comparable to the process image at 60 s from the polycarbonate slow test (10 mm $min^{-1}$). The measured maximum major true strain from the vision-based system is about 0.64, but the maximum major true strain obtained from ABAQUS [19] is about 0.25. One source of difficulty with the FEA method is that the current approach is not capable of modelling the exact necking and drawing behaviour of polycarbonate.

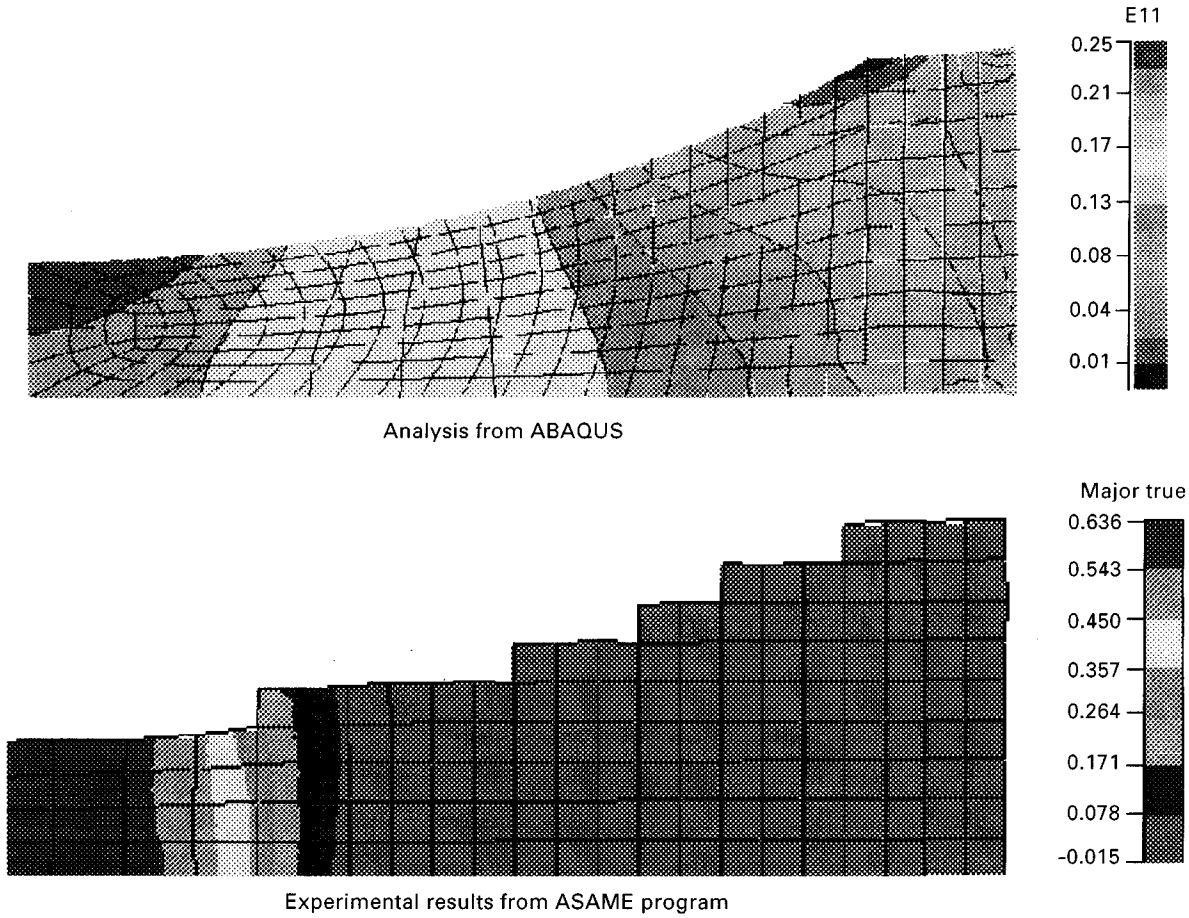


*Figure 9* Comparison of true major (longitudinal) strain distribution results obtained by finite element analysis (ABAQUS) and experimental results by vision-based system for polycarbonate hourglass specimen.

The entire neck initiation and propagation processes for 6111-T6 aluminium and polycarbonate are summarized in Fig. 10a and b. The engineering stress–strain behaviour of both materials is shown schematically in the figure. Key locations are labelled on each of the plots and a description of the necking process as related to these locations can be found below each plot.

Fig. 10a shows the engineering stress versus strain for 6111-T6 aluminium, and what happens to the specimen at these key locations on the stress–strain plot: how the neck initiates, how the neck further propagates, and the final fracture along the necked zone. Location (A) shows that localized bands are developing in the aluminium at approximately a 70° angle relative to the longitudinal axis of the specimen. The load is concentrated where these bands are developing, which initializes the localized neck. The narrow neck band is in plane strain along its longitudinal direction because it is constrained by the material above and below the neck [3]. The localization of deformation in the neck gives rise to load instability.

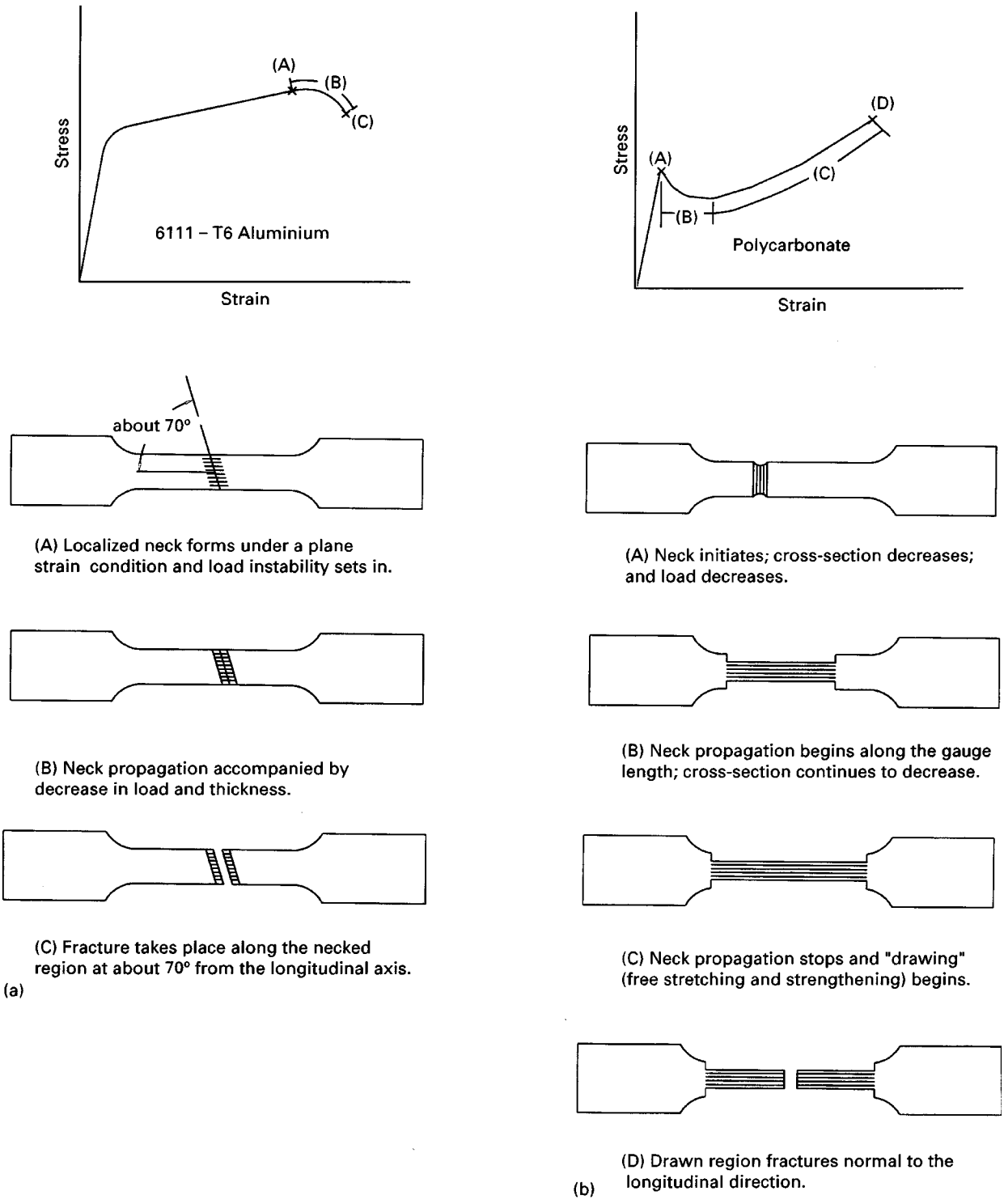


*Figure 10* Description of neck initial and propagation as related to the stress–strain plot for (a) the 6111-T6 aluminum specimens, and (b) the polycarbonate specimens.

At location (B) in Fig. 10a, the load decreases because the necked region has grown. The neck is propagating at this stage, as the load and the sample thickness are decreasing. The large strain rate sensitivity and the anisotropy of the 6111-T6 aluminium alloy helps distribute the strain better within the neck area and increase both the neck breadth and the neck extension to failure [7]. At location (C), the sample actually fractures because of the concentration of the localized bands.

Fig. 10b shows the engineering strain–strain curve for polycarbonate with key locations marked on the stress–strain plot. For polycarbonate, strain softening leads to a localization of plastic flow in bands or necks, because the decrease in load in the first part to pass its peak load reduces the load on the remainder of the specimen. Deformation is thus concentrated in the first region until it either hardens or breaks.

Location (A) shows that the molecules in the amorphous [5] polycarbonate are beginning to align themselves in the longitudinal direction. Crazes and voids [3] may develop as the sample is put into stress, and these will continue the necking process, thereby causing the load to drop. The voids can coalesce to form a crack, and eventually lead to fracture of the polymer. Deformation is thus concentrated in the first region until it either hardens or breaks. The cross-section of the gauge length decreases as the sample is stretched.

At location (B) of Fig. 10b, the neck is propagating throughout the gauge length of the sample and the sample is stretching such that its cross-section is decreasing. The load-carrying capacity of the specimen is dropping because, even though the necked area has been work hardened the most, this is offset by it having the smallest area. Orientation hardening effects are observed in the polycarbonate at large strains, along with significant strain softening after the yield point [5]. After initial yielding has taken place, further plastic deformation requires an increasing load but at a decreasing strain rate. Previous experimentation [9] showed that polycarbonate exhibited significant strain softening after yield and pronounced orientation hardening at large strains.

At location (C), neck growth stops as the neck now reaches the shoulders of the specimen. The specimen begins stretching and strengthening, also called "drawing" [18]. Finally, the specimen becomes so weak that it fractures at location (D). The fracture is normal to the longitudinal direction of the specimen because the molecules have been aligned in this longitudinal direction, making the sample weaker in this direction. Overall, the peak in the strain rate is in the neck and not at the point of highest strain [6].

The two crosshead testing speeds produced results that were quite similar except that the greater speed often resulted in fracture in less time because the load capacity of the sample reached its maximum faster. The hourglass samples that were tested without using the extensometer also produced similar results, but the final displacement was slightly greater for the hourglass samples that did not use the extensometer because the extensometer may have made small indentations on the specimen where it was clamped. Any small indentations on the specimen would have accelerated the necking process. The test was performed at the fast and slow speeds and with and without the extensometer simply to ensure that the data obtained by all methods was equivalent, and this did prove to be the case.

The longitudinal true strain to lateral true strain ratio for the hourglass samples is greater than two because of the geometrical constraints of these samples. Because the neck usually forms at the minimum width of the specimen, the area surrounding the neck is at a greater width. This creates a notch effect in which the strain at the neck region is distributed to the surrounding area and the lateral strain increases much slower than usual.

The assumed equivalence of the thickness and width strains proved to be approximately accurate. After fracture, the width and thickness of the samples were measured at specific locations on the specimen. These locations were chosen along lateral grid lines that were close to the fractured area. Using the initial width and thickness values together with the measured values after fracture, the true strain was calculated in both the width and the thickness directions. For the 6111-T6 aluminium alloy uniform specimen, the width true strain was determined to be about 0.66 times the thickness true strain. For the polycarbonate uniform specimen, the width true strain was approximately equal to 0.74 times the thickness true strain. These ratios of width true strain to thickness true strain show that the assumption of equivalent thickness and width true strains was approximately valid.

The net true strain on the sample, the sum of the longitudinal, width and thickness strains, was found to be equal to about zero, as predicted by the constant volume assumption. This net true strain was determined using the thickness and width true strains that were already measured. The longitudinal strain was obtained through the data in the ASAME program [10]. The major true strain values in the longitudinal direction were obtained for each of the centre four grid lines along the lateral grid line on which the thickness and width had been measured. These four longitudinal strain values were then averaged. The sum of the longitudinal, width, the thickness true strains for the particular grid line was calculated to be approximately zero, thereby confirming the acceptance of our assumption of volume constancy in the specimen.

Several significant observations have been made from the present work. The first is that the vision-based measurement gives accurate strain measurement when compared to the extensometer data. The second is that localized deformation develops principally in the longitudinal direction and propagates in this direction, in which the load is applied. Some non-uniformity in strain distribution is observed in the minor strain in the lateral direction. Also, the major and minor strain in the longitudinal direction peaks in the centre of the hourglass specimen.

The third observation is that a neck develops at an angle of about 70° from the longitudinal axis and

fractures along that direction for 6111-T6 aluminium. Comparatively, the neck and fracture line are always oriented 90° from the loading (longitudinal) direction for polycarbonate. The fourth result is that the longitudinal strain is more than twice the lateral strain in the hourglass samples. This is because as the smallest section of the neck elongates under continued displacement, its lateral contraction is restrained by adjacent sections that are more lightly stressed because they are a little larger. This constraint causes lateral tension in the neck, where these stresses increase from zero at the surface to a maximum at the interior. To maintain flow, the longitudinal strain increases to a maximum at the centre of the hourglass specimen in the longitudinal direction, as shown in Fig. 7b and d.

## 5. Conclusions

1. The vision-based method, consisting of the ASAME program [10] and the CCD camera, is effective in accurately determining the strain distribution. With gridded specimens, neck initiation and propagation can be characterized in both the longitudinal and the lateral directions. This vision-based system produced improvements over previously published results because of its ability to accurately measure the longitudinal and lateral true strain at all of the grid points in both the longitudinal and lateral directions.

2. Neck initiation can be determined by examining the strain distribution as the sample is pulled in tension. Measurements of the distance that the deforming section of the specimen elongates, together with time records, can be used to determine the velocity of neck propagation in the specimen. The photographs of the specimens after fracture show that polycarbonate fractures at an angle of 90° and 6111-T6 aluminium at an angle of about 70° with respect to the longitudinal axis of the specimen.

3. The longitudinal true strain to lateral true strain ratio is greater than 2:1 for the hourglass specimens because of their geometrical constraints. For aluminium, the ratio is about 3.1:1 and for polycarbonate, the ratio is about 5.1:1. The longitudinal to lateral true strain ratio is about 2:1 for the uniform section specimens.

4. For both the 6111-T6 aluminium and the polycarbonate, the major (longitudinal) and minor (lateral) strains are uniform across the majority of the gauge length of the uniform section specimens in the longitudinal direction. For both the 6111-T6 aluminium and the polycarbonate, the major and minor strains peak at the centre of the hourglass specimens in the longitudinal direction. The major strain is uniform, however, the minor strain is non-uniform in the lateral direction for the uniform section and the hourglass specimens for both materials.

## Acknowledgements

The sheet test samples were silk-screened with the help of Rebecca Pearce and the ASAME vision-based data acquisition [10] and processing software was provided by David Manthey of CamSys, Inc., Troy, NY. Keith Knapp set up the data acquisition software, initialized the FEA geometry file, and made many useful suggestions for the experimental procedure and its documentation.

## References

1. F. HOSFORD and R. M. CADDELL, in "Metal Forming", (PTR Prentice Hall, Englewood Cliffs, NJ, 1993) pp. 49–61.
2. A. McCLINTOCK and A. S. ARGON, in "Mechanical Behavior of Materials", (Addison-Wesley Publishing Company, Inc., Reading, MA, USA, 1966) pp. 312–316, 321.
3. S. KALPAKJIAN, in "Manufacturing Processes for Engineering Materials", (Addison-Wesley, Reading, MA, USA, 1984) pp. 386–652.
4. N. HAWARD, *Polymer* **28** (1987) 1485.
5. J. AMODEO and D. LEE, *Polym. Engng. Sci.* **32** (1992) 1055.
6. A. R. HAYNES and P. D. COATES, *J. Mater. Sci.* **31** (1996) 1843.
7. K. GHOSH, *Metall. Trans.* **5** (1974) 1607.
8. D. W. MANTHEY and D. LEE, *J. Met.* **47** (1995) 46.
9. D. LEE and P. C. LUKEN, *Polym. Engng. Sci.* **26** (1986) 612.
10. "ASAME Automated Strain Analysis and Measurement Environment Users Manual" (CamSys, Inc., Troy, NY, USA, 1997).
11. "NI-DAQ Function Reference Manual Version 4.6.1" (National Instruments Corp., Austin, TX, USA, 1994).
12. "LabVIEW Networking Reference Manual" (National Instruments Corp., Austin, TX, USA, 1994).
13. J. H. VOGEL and D. LEE, *J. Met.* **42** (1990) 8.
14. S. M. METWALLI, A. R. RAGAB, A. H. KAMEL and A. A. SAHEB, *Exp. Mech.* **27** (1987) 414.
15. J. S. SIRKIS and C. E. TAYLOR, *ibid.* **30** (1990) 26.
16. J. S. SIRKIS and T. J. LIM, *ibid.* **31** (1991) 382.
17. K. D. MAZACHEK and T. N. FADDIS, *J. Test. Eval.* **20** (1992) 121.
18. P. D. COATES and I. M. WARD, *J. Mater. Sci.* **15** (1980) 2897.
19. "ABAQUS Theory Manual" (Habbitt, Karlsson, and Sorensen, Inc., Providence, RI, USA, 1995).
20. P. D. COATES, R. G. SPEIGHT and A. R. HAYNES, *Polymer* **35** (1994) 383.

*Received 18 August 1997*
*and accepted 13 February 1998*